Polymer Journal (2011) 43, 293–300

www.nature.com/pj

ORIGINAL ARTICLE

Denaturant-induced helix–coil transition of oligopeptides: theoretical and equilibrium studies of short oligopeptides C17 and AK16

Fumiaki Kanô[1,5], Masaji Shinjo[2,5], Zhi-jie Qin[2,6], Jinsong Li[2], Yoshitaka Matsumura[2], Akio Shimizu[3], Akio Teramoto[4,*] and Hiroshi Kihara[2]

A statistical mechanical theory on the effects of denaturant on the helix–coil transition of polypeptides was developed. In the proposed theory, unfolding agents were assumed to interact with the polypeptide backbone. The theoretical results were compared with the findings of guanidine-induced helix–coil transition experiments, which were conducted on short peptides (C17 and AK16). Specifically, the helix fraction and average number of helices in C17 and AK16 were estimated. Under unfolding conditions (high denaturant concentration), the number of helices in a given sequence was close to zero. The radius of gyration was measured, and the results were related to those of the proposed theory.
Polymer Journal (2011) **43,** 293–300; doi:10.1038/pj.2010.143; published online 2 February 2011

Keywords: AK16; C17; helix–coil transition; α-helix; protein denaturation; unfolding by denaturant; Zimm–Bragg theory

INTRODUCTION

The α-helix is an important structural unit that is commonly found in proteins. α-Helices can transform into the coiled state based on the temperature, pH and the concentration of denaturants, such as urea and guanidium salts. Helix–coil transitions of polypeptides have been extensively studied by Zimm and Bragg,[1] Nagai[2] and Lifson and Roig[3] (see for reviews[4,5]).

In this study, we developed a denaturant-induced helix–coil transition theory based on statistical physics. Denaturant-induced protein unfolding was initially studied by Tanford *et al.* (see for reviews ref.[6,7]) and has been extensively investigated by many other researchers (see for reviews ref.[8,9]). However, the mechanism of unfolding has not yet been elucidated. One possible mechanism of denaturant-induced protein unfolding involves a change in the solvent properties of water. These effects could alter the packing interactions of α-helices and β-sheets. Another possible mechanism may include specific interactions with functional groups on the protein. In fact, the interaction of denaturants with nonpolar and polar surfaces is more favorable than that of water. Interactions between the denaturant and the peptide backbone disturb hydrogen bonds in water and the interior of the protein. Thus, to understand the unfolding of α-helices in proteins by denaturants, interactions between the denaturant and the peptide backbone must be understood.

Schellman[10,11] developed a protein unfolding theory based on the selective solvation of denaturants thermodynamically. Using Schellman's theory, the effects of denaturants on helix–coil transitions have been studied by Scholtz *et al.*,[12] who connected the thermodynamic solvation model derived by Schellman[10,11] to the Zimm and Bragg model for the analysis of the unfolding of peptide helices by urea. However, the method was phenomenological and was not consistently based on statistical physics.

For the helix–coil transition, two types of theory based on the transfer-matrix method have been used to explain the molecular mechanism of these phenomena. Hydrogen bonds were evaluated in one theory,[1] and the other theory considered residue conformations.[3] Nagai[2] developed these treatments into a new theory based on the spatial conformation of the helix.

In this study, we developed a new denaturant-induced helix–coil transition theory through a propagator method. The proposed theory is easy to handle, and the physical averaged quantities are simple to calculate.[13–15] Moreover, the effect of denaturants on the statistical weight was considered. The grand partition function was calculated, and averaged quantities, such as the helix fraction, number of helices and end-to-end distance of the polypeptide, were derived as a function of the denaturant concentration.

We analyzed the guanidine hydrochloride (GuHCl)-induced helix–coil transition of short peptides (C17 and AK16) according to the proposed theory. C17 consists of DLTDDIMCVKKILDKVG, corresponding to α-helical region of the 84th to 100th amino acid

[1]Department of Physics, Showa University, 4562 Kamiyoshida, Fujiyoshida, Japan; [2]Department of Physics, Kansai Medical University, Hirakata, Japan; [3]Department of Environmental Engineering, Symbiosis Faculty of Engineering, Soka University, Hachioji, Japan and [4]Faculty of Science and Engineering, Ritsumeikan University, Shiga, Japan
[5]These two authors contributed equally to this work.
[6]Current address: Department of Chemistry and Biochemistry, University of California at Santa Cruz, Santa Cruz, CA 95064, USA.
*This paper is dedicated to Akio Teramoto, who passed away on 7 February 2010.
Correspondence: Professor H Kihara, Department of Physics, Kansai Medical University, 18-89 Uyama-Higashi, Hirakata 573-1136, Japan,
E-mail: kihara@makino.kmu.ac.jp
Received 17 August 2010; revised 10 November 2010; accepted 22 November 2010; published online 2 February 2011

of bovine α-lactalbumin. Alternatively, AK16 consists of Ac-YGAA-KAAAAKAAAAKA-NH2.

THEORY

Statistical analysis of helix–coil transitions induced by denaturant

Treatment by Doi[14] can be extended to include the effects of denaturation by denaturants. We assumed that the denaturant molecules only bind to the coil of the polypeptide and that the surface of the helix becomes unavailable for binding.

For each coiled portion of n peptide units (residues), the statistical weight between the start point r and the end point r' can be expressed as

$$G_c(\boldsymbol{r}-\boldsymbol{r}',n,m)=\binom{pn}{m}q^m H_c(\boldsymbol{r}-\boldsymbol{r}',n) \tag{1}$$

with

$$H_c(\boldsymbol{r},n)=\exp\left(-\frac{\Delta g}{k_B T}n\right)\left(\frac{2\pi n b^2}{3}\right)^{-3/2}\exp(-\frac{3\boldsymbol{r}^2}{2nb^2}) \tag{2}$$

where m is the number of residues that are attached to denaturant molecules, p is the maximum number of attached denaturant molecules per residue, q is the partition function, which is dependent on the internal degree of freedom of denaturant molecules attached to a residue, b is the effective bond length of the residue, Δg is the difference in the free energy of the coiled and helical portion of the residue (which implies that all free energies are measured from the complete helix state), k_B is the Boltzmann constant and T is the absolute temperature.

For the helical portion of n peptide units, the statistical weight between point $\boldsymbol{r}$ and point $\boldsymbol{r}'$ can be expressed as

$$G_h(\boldsymbol{r}-\boldsymbol{r}',n)=\frac{\delta(|\boldsymbol{r}-\boldsymbol{r}'|-na)}{4\pi n^2 a^2} \tag{3}$$

where a is the length of the bond projected onto the helical axis.

We assumed that both ends of the peptide were in the coiled state; thus, the statistical weight of the system, which consists of N peptide units and end-to-end vector $\boldsymbol{R}$, can be written as

$$\begin{aligned}Q(\boldsymbol{R},N,\lambda)=&\int d^3r_1 dn_1 \sum_{m_1=0}^{n_1}\binom{pn_1}{m_1}(q\lambda)^{m_1}H_c(r_1,n_1)\\&+v^2\iint d^3\boldsymbol{r_1}dn_1 d^3r_2 dn_2\sum_{m_1=0}^{n_1}\binom{pn_1}{m_1}(q\lambda)^{m_1}H_c(\boldsymbol{r_1},n_1)\\&\times G_h(\boldsymbol{r_2},n_2)\times\sum_{m_3=0}^{n_3}\binom{pn_3}{m_3}(q\lambda)^{m_3}H_c(\boldsymbol{r_3},n_3)\\&+\cdots=\sum_{i=0}^{\infty}v^{2i}\int d^3\boldsymbol{r_1}dn_1\cdots\int d^3\boldsymbol{r}_{2i}dn_{2i}(1+q\lambda)^{p(n_1+n_3+\cdots+n_{2i+1})}Q_1\end{aligned} \tag{4}$$

with

$$Q_1=H_c(\boldsymbol{r_1},n_1)G_h(\boldsymbol{r_2},n_2)\cdot\cdot H_c(\boldsymbol{r}_{2i+1},n_{2i+1}) \tag{5}$$

where v is the statistical weight of the boundary between the random coil sequences and the helix, at which there is a lack of hydrogen bonding, and λ is the absolute activity of the denaturant molecule. The value of the parameter v was identical to that assigned to the helix termini by Lifson and Roig.[3] Because N is a large number, n_i is considered as a continuous number and can be integrated. All possible compositions must be counted under the conditions that the total number of peptide units is equal to N and that the length of the end-to-end vector is equal to $\boldsymbol{R}$. To avoid this complication, Laplace transforms and Fourier transforms were conducted on N and $\boldsymbol{R}$, respectively.

$$\begin{aligned}\hat{Q}(\boldsymbol{k},\omega,\lambda)&=\int_0^{\infty}dSe^{-\omega S}\int Q(\boldsymbol{R},S,\lambda)e^{-ik\boldsymbol{R}}d^3R\\&=\frac{G_c(\boldsymbol{k},\omega,\lambda)}{1-v^2G_c(\boldsymbol{k},\omega,\lambda)G_h(\boldsymbol{k},\omega)}\end{aligned} \tag{6}$$

with

$$G_c(\boldsymbol{k},\omega,\lambda)=(\omega+\epsilon+\frac{b^2k^2}{6})^{-1} \tag{7}$$

$$G_h(\boldsymbol{k},\omega)=-\frac{1}{2ika}\ln\frac{i\omega+ka}{i\omega-ka} \tag{8}$$

$$\epsilon=\epsilon_0-p\ln(1+q\lambda) \tag{9}$$

$$\epsilon_0=\frac{\Delta g}{k_B T} \tag{10}$$

$$\lambda=\frac{\beta}{q_s}C',\quad \beta=\frac{M_w}{10^3\gamma M_s} \tag{11}$$

ϵ is the reduced free energy difference between the coiled and helix portion of the residue, and ϵ_0 is the ϵ-value of the residue in the absence of the denaturant. q_s is the partition function originating from the internal degree of freedom of the denaturant molecule in solution, M_w and M_s are the molecular weight of water and the denaturant, respectively, and γ ($g\,l^{-1}$) and C' ($mg\,l^{-1}$) are the density of the solution and the concentration of solute, respectively.[16]

Thus, the statistical weight of a system composed of N peptide units can be obtained by reverse transforming Equation (6).

$$\begin{aligned}\hat{\hat{Q}}(\boldsymbol{k},N,\lambda)&=\frac{1}{2\pi i}\int_{d-i\infty}^{d+i\infty}e^{\omega N}\hat{Q}(\boldsymbol{k},\omega,\lambda)d\omega\\&=\int Q(\boldsymbol{R},N,\lambda)e^{-i\boldsymbol{kR}}d^3R\\&=\Xi(N,\lambda)(1-\frac{k^2}{6}<R^2(N,\lambda)>+\cdots)\end{aligned} \tag{12}$$

where d is a real number that is larger than the real part in any pole of $\hat{Q}(\boldsymbol{k},\omega,\lambda)$ in the ω plane. The grand partition function $\Xi(N,\lambda)$ of a system composed of N units can be expressed as

$$\begin{aligned}\Xi(N,\lambda)&=\hat{\hat{Q}}(\boldsymbol{k}=0,N,\lambda)\\&=\frac{1}{2\pi i}\oint_C e^{\omega N}\hat{Q}(\boldsymbol{k}=\boldsymbol{0},\omega,\lambda)d\omega\end{aligned} \tag{13}$$

The integral in Equation (12) transforms into the contour integral, including the poles. The contour of the integral of C is shown in Figure 1:

$$\Xi(N,\lambda)=\frac{\omega_+e^{\omega_+N}-\omega_-e^{\omega_-N}}{\omega_+-\omega_-} \tag{14}$$

with

$$\omega_{\pm}=\frac{-\epsilon\pm\sqrt{\epsilon^2+4v^2}}{2} \tag{15}$$

Our parameters correspond approximately to the Zimm–Bragg parameters and the Lifson–Roig parameters:[1,3,4]

$$e^{\epsilon}=s=\frac{w}{1+v} \tag{16}$$

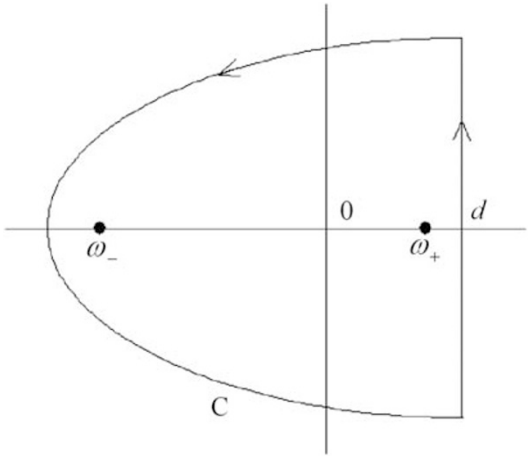

Figure 1 Graphical representation of the contour of integral *C* of Equation (13).

$$\sigma = \frac{v^2}{(1+v)^4} \tag{17}$$

where s and σ are the helix propagation parameter and the helix nucleation parameter, respectively, and w is a parameter of the Lifson–Roig model and is a weight assigned to helical residues in the interior of the helix.

We refer to the quantity $q\lambda$ as the denaturant molarity. According to its definition, we can transform Equation (11) into the following expression:

$$q\lambda = \eta C \tag{18}$$

where C is the denaturant molarity and η is the coefficient of C, which can be expressed as

$$C = \frac{C'}{10^3 Ms} \tag{19}$$

$$\eta = \frac{M_W}{\gamma}\frac{q}{q_s} \tag{20}$$

The dependence of the helical structure on the molarity of the denaturant can be used to quantify the effects of the denaturant on the unfolding of the helix. The reduced free energy, ϵ, was calculated according to Equation (9) and is plotted in Figure 2 as a function of the denaturant molarity at various values of p. The value of ϵ in the transition range decreased almost linearly as the value of C increased.

Average quantities

Ratio of peptides in the helix state: $\boldsymbol{f}_{\mathrm{H}}$. Based on Equation (14), f_{H} was obtained from the following equation:

$$\begin{aligned} f_{\mathrm{H}} =& 1+\frac{1}{N}\frac{\partial \ln \Xi}{\partial \epsilon} \\ =& \frac{1}{2}\left(1+\frac{\epsilon}{\sqrt{\epsilon^2+4v^2}}\right)+\frac{1}{2NA}\times\left[-1+e^{-(\omega_+-\omega_-)N}\right. \\ &+\left\{1+(1+2N\omega_-)e^{-(\omega_+-\omega_-)N}\right\} \\ &\left.\times\frac{\epsilon}{\sqrt{\epsilon^2+4v^2}}\right]-\frac{\epsilon}{N(\epsilon^2+4v^2)} \end{aligned} \tag{21}$$

with

$$A = \omega_+ - \omega_- \times e^{-(\omega_+-\omega_-)N} \tag{22}$$

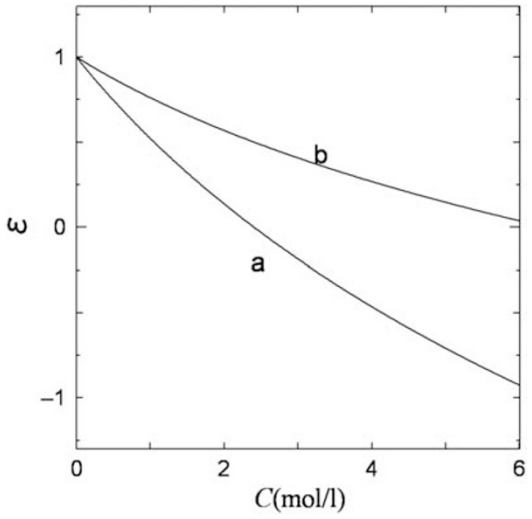

Figure 2 Dependence of the reduced free energy, ϵ, on the denaturant molarity. The numerical values were ϵ_0=1.0 and η=0.27. For a and b, p=2 and 1, respectively.

Average number of units in the helix state: $\boldsymbol{i}_{\mathrm{H}}$. Based on Equation (14), i_{H} was obtained from the following equation:

$$\begin{aligned} i_{\mathrm{H}} =& \frac{\partial \ln \Xi}{\partial \ln v^2} = \frac{v^2}{\sqrt{\epsilon^2+4v^2}} \\ &\times\left[N+\frac{1}{A}\left\{1+(1+2N\omega_-)e^{-(\omega_+-\omega_-)N}\right\}-\frac{2}{\sqrt{\epsilon^2+4v^2}}\right] \end{aligned} \tag{23}$$

Mean square end-to-end distance of a peptide: $\langle R^2 \rangle$. Based on Equation (14), $\langle R^2 \rangle$ was obtained from the following equation:

$$\begin{aligned} \langle R(N)^2 \rangle =& -\frac{6}{\Xi(N,\lambda)}\lim_{k\to 0}\frac{\partial Q(\boldsymbol{k},N,\lambda)}{\partial k^2} \\ =& -\frac{6}{\Xi(N,\lambda)}\times\frac{1}{2\pi i}\int_{d-i\infty}^{d+i\infty} e^{\omega N}\frac{b^2\omega^3+2v^2a^2}{\omega(\omega^2+\epsilon-v^2)}d\omega \\ =& -\frac{6}{\Xi(N,\lambda)}\left\{(B+DN+BN\omega_+)e^{\omega_+ N}\right. \\ &\left.+(E+FN+EN\omega_-)Ne^{\omega_- N}+\frac{G}{6}\right\} \end{aligned} \tag{24}$$

where

$$B = \frac{\omega_+\omega_-^2 G+4\omega_-(\omega_+-\omega_-)D}{2\omega_+\left(\omega_-^2-\omega_+^2\right)} \tag{25}$$

$$D = \frac{\frac{\epsilon b^2}{2}+\left(2\omega_-^2-\frac{\omega_-^3}{\omega_+}\right)G}{3(\omega_+-\omega_-)^3}\omega_+^2 \tag{26}$$

$$E = -B-\frac{G}{6} \tag{27}$$

$$F = -\frac{2a^2\epsilon}{3\omega_+^2}-\left(\frac{\omega_-}{\omega_+}\right)^2 D \tag{28}$$

$$G = -2\left(\frac{a}{v}\right)^2 \tag{29}$$

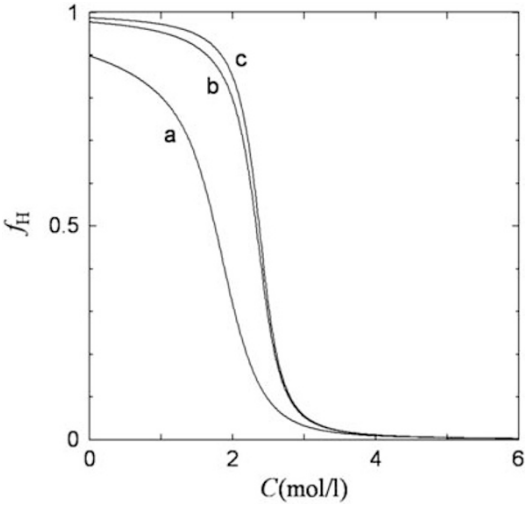

Figure 3 The fraction of the helix state, f_H, as a function of the denaturant molarity, *C*. The curves were drawn according to Equation (21). The numerical values were v=0.05, ϵ_0=1.0, η=0.27 and p=2. N=20 for a, N=100 for b and N=200 for c.

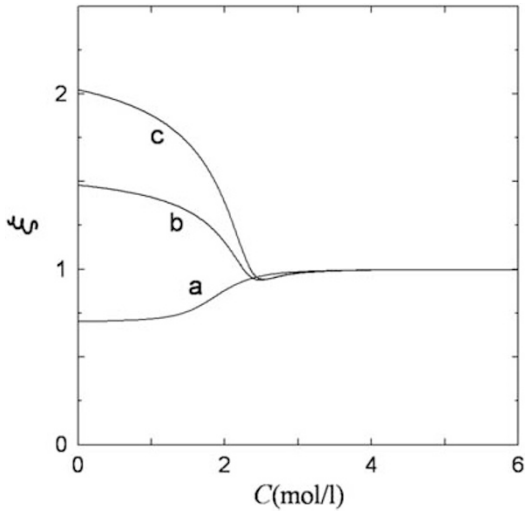

Figure 5 The value of ξ, the root mean square end-to-end distance divided by $\sqrt{Nb^2}$ as a function of *C*, according to Equation (24). The numerical value of b/a=10. The values of the other parameters are identical to those shown in Figure 3.

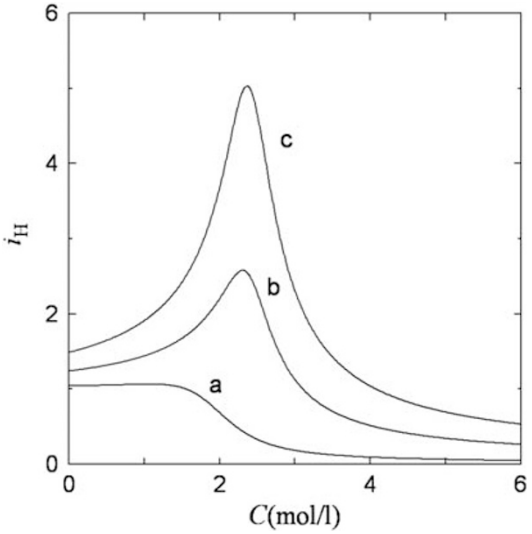

Figure 4 The number of helices as a function of *C*. The curves were drawn according to Equation (23). The numerical values of the parameters are identical to those in Figure 3.

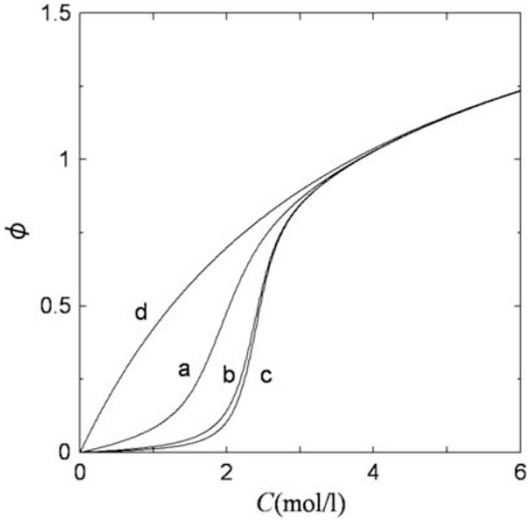

Figure 6 Dependence of ϕ on the denaturant molarity. The curves were drawn according to Equation (30). The numerical values for the parameters are identical to those shown in Figure 3. The other numerical values for d are v=0.05, ϵ_0 =−0.10, η=0.27, p=2 and N=20.

In Figures 3–5, the following quantities are shown as a function of the solvent molarity (*C*): the ratio of peptide in the helix state (Figure 3), the average number of helix (Figure 4) and the root mean square end-to-end distance divided by $\sqrt{Nb^2}$, $\xi=\sqrt{\langle R(N)^2\rangle/Nb^2}$ (Figure 5). The results shown in the figures clearly demonstrate that the helix content and the average number of helix change near the transition point, $\epsilon\sim0$. The transition becomes sharper as the number of residues increases. This property is closely related to the fact that a minimum is observed when the radius of gyration is plotted as a function of solution condition.[17] In a short peptide, there is zero or one helix through out the transition process, as shown in Figure 4. The helix moves forward or backward due to the winding and unwinding process at both ends of the chain[18] and is attacked by denaturant molecules.

Degree of denaturant binding: $\boldsymbol{\phi}$. The ratio of the number of denaturant molecules bound to a residue can be expressed as

$$\phi=\frac{1}{N}\frac{\partial\ln\Xi}{\partial\ln\lambda}=\frac{pq\lambda}{1+q\lambda}(1-f_H) \qquad (30)$$

The fraction 1–f_H is the degree of residues in the random coiled state. Although the formation of intramolecular hydrogen bonds is a cooperative phenomena, the degree of denaturant binding is given as the product of the coil fraction (1–f_H) and the coverage of the Langmuir isotherm. The characteristics of ϕ in Equation (30) were nearly identical to the results obtained by Bixon and Lifson.[19] In Figure 6, notable features of the system are revealed. For instance, when the initial state of the peptide is helical ($\epsilon_0>0$), the degree of denaturant binding (ϕ) produces a sigmoidal curve. Under these conditions, ϕ can be attributed to the coil fraction, 1–f_H. Alternatively,

when the initial state of the peptide is coiled ($\epsilon_0<0$), ϕ demonstrates Langmuir-type binding.

Helix fraction and number of the Lifson–Roig model

If v^2 is small, Equation (17) can be approximated as

$$v^2=\sigma \tag{31}$$

In this case, f_H and i_H can be approximated as

$$\begin{aligned} f_H=& \\ & f\left\{1-\frac{2\sqrt{f(1-f)}}{N\sigma^{1/2}}+\left[1+\frac{2\sqrt{f(1-f)}}{N\sigma^{1/2}}\right]\right. \\ & \left.\times\exp\left[-\frac{N\sigma^{1/2}}{\sqrt{f(1-f)}}\right]\right\} \\ & \times\left\{1+\left(\frac{f}{1-f}\right)\exp\left[-\frac{N\sigma^{1/2}}{\sqrt{f(1-f)}}\right]\right\}^{-1} \\ =& f(1-f)\left\{1-\frac{2}{NP}+\left(1+\frac{2}{NP}\right)e^{-NP}\right\} \\ & \times\left(1-f+fe^{-NP}\right)^{-1} \end{aligned} \tag{32}$$

and

$$\begin{aligned} i_H=& f(1-f)\left(\frac{N\sigma^{1/2}}{\sqrt{f(1-f)}}-2\right) \\ & +f\left\{1+\left(1-\frac{2Nf\sigma^{1/2}}{\sqrt{f(1-f)}}\right)\exp\left[-\frac{N\sigma^{1/2}}{\sqrt{f(1-f)}}\right]\right\} \\ & \times\left\{1+\left(\frac{f}{1-f}\right)\exp\left[-\frac{N\sigma^{1/2}}{\sqrt{f(1-f)}}\right]\right\}^{-1} \\ =& f(1-f)\left[NP-2+\left\{1+(1-2fNP)e^{-NP}\right\}\right. \\ & \left.\times\left(1-f+fe^{-NP}\right)^{-1}\right] \end{aligned} \tag{33}$$

where

$$f=\frac{1}{2}\left(1+\frac{\epsilon}{\sqrt{\epsilon^2+4v^2}}\right)=\frac{1}{2}\left[1+\frac{\ln s}{\sqrt{(\ln s)^2+4\sigma}}\right] \tag{34}$$

and

$$P=\frac{\sigma^{1/2}}{\sqrt{f(1-f)}} \tag{35}$$

Equation (32) is equal to the equation obtained by Teramoto.[20]

EXPERIMENTAL PROCEDURE

Circular dichroism (CD) was conducted on an UNISOKU (Unisoku Inc., Hirakata, Osaka, Japan) spectropolarimeter, and the C17 and AK16 peptides were synthesized according to standard procedure (AS).

For the CD measurements, C17 and AK16 peptides were dissolved in a mixture of 0.01 M phosphate buffer (30%) and methanol (70%). For C17 and AK16, the pH of the buffer was set to 2.0 and 7.0, respectively, and the measurements were conducted at –40 °C.

X-ray scattering experiments were performed on C17 at the beam line 15A small angle installation (BL-15A) of the Photon Factory at High Energy Acceleration Research Organization (KEK), Tsukuba, Japan. A stable beam of photons with a wavelength of 1.50 Å was provided by a horizontally focusing bent-crystal monochromator and a vertically focusing mirror.[21] Scattering data were obtained with a CCD-based X-ray detector (Hamamatsu Photonics K.K., Hamamatsu, Japan)[22] and corrected for image distortion, nonuniform sensitivity and contrast reduction with an X-ray image intensifier before the analysis.[23,24] The detector was set at a distance of 1000 ± 10 mm from the sample. The concentration of peptides was set to 1 mg ml^{-1}, and the temperature was maintained at 25 °C. A 0.01 M phosphate buffer in 70% methanol at pH 2.0 was used.

ANALYSIS

According to the proposed theory, f_H can be expressed as Equation (21). The parameter ϵ was converted into s by Equation (16), and s was related to the denaturant concentration C:

$$\frac{1}{s}=\frac{(1+\eta C)^p}{s_0} \tag{36}$$

where

$$s_0=\exp\left(\frac{\Delta g}{k_B T}\right) \tag{37}$$

Thus, ϵ and C are directly related through s, and f_H can be expressed as a function of C.

f_H can be obtained from CD observations by using the following expression:

$$f_H=\frac{\theta-\theta_C}{\theta_H-\theta_C} \tag{38}$$

where θ is the mean residue ellipticity at 222 nm as a function of C, and θ_C and θ_H are the θ-values of the coiled and helix state, respectively. θ_C and θ_H are also dependent on the denaturant concentration:[25]

$$\begin{aligned} \theta_C=&\theta_{C0}+d_c C \\ \theta_H=&\theta_{H0}+d_h C \end{aligned} \tag{39}$$

where θ_{C0} and θ_{H0} are the values of θ_C and θ_H at a denaturant concentration of 0 M, respectively. d_c and d_h are constants.

The θ-values were fitted to the CD data by parameter fitting.

In the fitting analysis, θ_{C0} was set to 640 (deg cm^{-2} dmol^{-1})[26] for both peptides. θ_{H0} was estimated from the fitting calculation, along with s_0 and η. d_c and d_h were estimated from the experimental data presented in the Results section.

A two-state equilibrium was also considered:

$$[N]+m'[D]\leftrightharpoons[U-m'D]K=\frac{[U-m'D]}{[N][D]^{m'}} \tag{40}$$

where [N] is the concentration of the peptide in the native state, [D] is the concentration of the denaturant, m' is the number of bound denaturant molecules to an unfolded oligopeptide, [U–m'D] is the concentration of unfolded denaturant-bound oligopeptide and K is the equilibrium constant.

For this reaction, L_θ was expressed according to the following equation:

$$L_\theta=\frac{L_H+K[D]^{m'}L_U}{1+K[D]^{m'}} \tag{41}$$

where L_H and L_U are the CD values of the native and denatured states, respectively.

RESULTS

The CD experiments were conducted on C17 and AK16 peptides, and the results are shown in Figures 7a and b. As shown in the figures, C17 and AK16 are present in the random coil form at high GuHCl concentrations. The θ_{222} values of the native and coiled states were linearly proportional to the GuHCl concentration. The transition curve was fitted to Equation (41), as shown in Figures 7a and b. For C17, K=0.04 and m'=5.3. Alternatively, for AK16, K=0.0004 and m'=7.6. The experimental data shown in Figures 7a and b were also

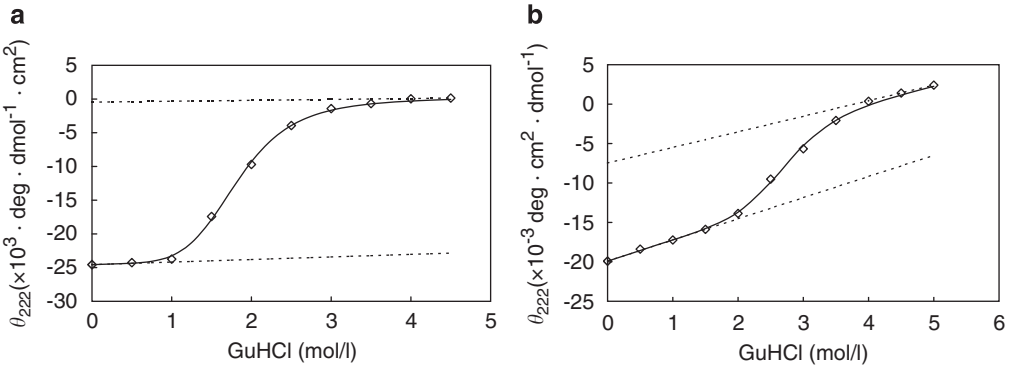

Figure 7 The experimental circular dichroism results. θ_{222} versus the guanidine hydrochloride (GuHCl) concentration. The solid line represents the fit of Equation (41). The measurements were conducted at −40 °C in the presence of 70% methanol at pH 2.0 and 7.0 for C17 and AK16, respectively. (**a**) C17 and (**b**) AK16.

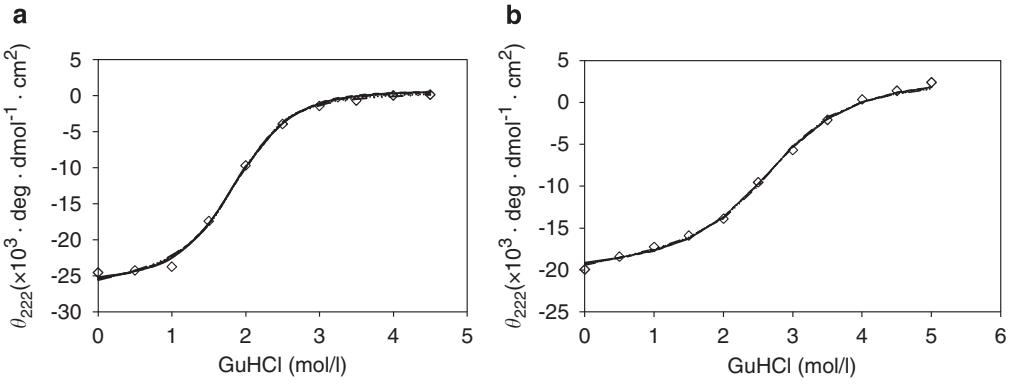

Figure 8 Experimental circular dichroism results. The fitted lines were obtained from statistical theory (Equations 16, 21, 36 and 38). (**a**) C17 and (**b**) AK16. In both figures, six fitted lines were drawn at $v^2=10^{-2}$, 10^{-3} and 10^{-4}, and $p=1$ and 2. The six fitted lines nearly overlap.

simulated according to statistical theory (Equations 16, 21, 36 and 38). According to Equation (38), θ is considered a function of f_H, and f_H is a function of C through ϵ and s, as described in the Analysis section. For C17, we adopted $d_c=d_h=0$ because the data were nearly constant at high and low concentrations of denaturant. For AK16, we used $d_c=d_h=0.354$; d_c was estimated from two data points, θ_{C0} and θ value at a denaturant concentration of 5 M, and the same value was also used for d_h. The results shown in Figures 8a and b were obtained from the fitting curves and were calculated at various v^2 and p-values. For all of the p- and v^2-values, the model provided a satisfactory fit to the experimental data. p is the number of denaturant-attachable sites per coiled residue and was assumed to be equal to 1 or 2, based on the chemical structure of the peptide residue. Subsequently, the experimental and theoretical values of $1/s$ were compared. Figure 9 shows a plot of $1/s$ versus the GuHCl concentration at $v^2=10^{-4}$. To estimate the optimal v^2-value, the standard deviation (Δ) was calculated at various v^2-values:

$$\Delta = \sqrt{\frac{\sum \Delta_i^2}{n'}} \tag{42}$$

where Δ_i is the difference between the fitted line and the experimental data at each concentration, and n' is the number of data points. In Figure 9 (inset), Δ is shown as a function of v^2. For AK16, Δ decreased and became nearly constant when v^2 was $<10^{-3}$. Moreover, for C17, Δ decreased when $v^2=10^{-4}$. On the basis of the results described in the literature, 10^{-3} to 10^{-4} are reasonable values for v^2;[20,26,27] thus, $v^2=10^{-4}$ was used in subsequent analyses. The difference between $p=1$ and $p=2$ was not significant; thus, because similar results were obtained when $v^2=10^{-3}$, the data shown hereafter were obtained at $v^2=10^{-4}$. For C17, s_0 was 2.4–2.6, η was 0.14–0.34 and θ_{H0} was $-29\,000$ ($\mathrm{deg\,cm^{-2}\,dmol^{-1}}$) when $p=1$ and $p=2$. For AK16, s_0 was 2.6–2.8, η was 0.09–0.26 and θ_{H0} was $-22\,000$ ($\mathrm{deg\,cm^{-2}\,dmol^{-1}}$) when $p=1$ and $p=2$. In both cases, these s_0 values were greater than that ($s_0=1.39$) reported by Scholtz *et al.*[12]

As shown in Figure 10, f_H was calculated from the fitted curve, and the experimental data shown in Figure 8 were plotted against C for C17 and AK16. At a GuHCl concentration of 0 M, the proportion of the helix form of the peptide was >85%, which indicates that all of the residues in the peptide formed a helix, except for the residues located at the ends of the peptide. The average number of helices in one sequence was calculated according to Equation (23), and the results are shown in Figure 11. On the basis of the results shown in this figure, short peptides such as C17 and AK16 do not contain plural helices in the helix–coil transition region. Moreover, the average number of helices was nearly zero at higher GuHCl concentrations. With C17, the average number of helices was equal to 0.08 at a GuHCl concentration of 3.5 M. Thus, 92% of C17 molecules were not in the helix form under these conditions.

Radius of gyration of C17

X-ray solution scattering was performed on C17, and the radius of gyration (R_g) was plotted against the GuHCl concentration (Figure 12). R_g=9.5 Å (R_H) at low GuHCl concentrations, and R_g =12.8 Å (R_U) at high GuHCl concentrations.

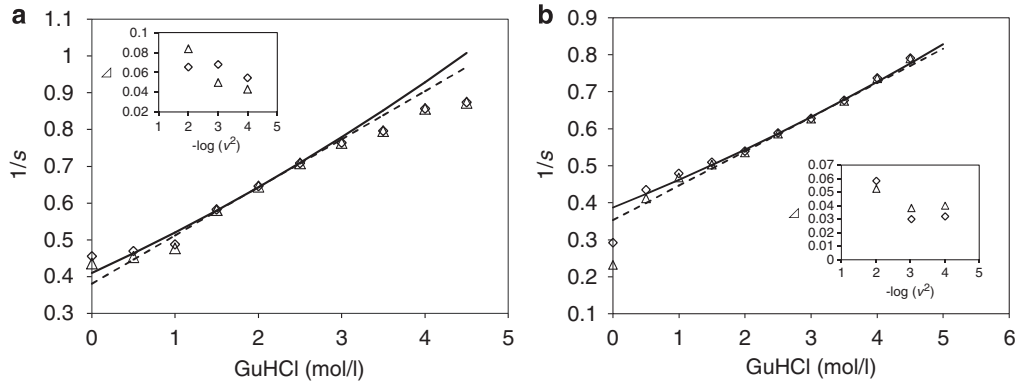

Figure 9 $1/s$ ($v^2=10^{-4}$) versus the guanidine hydrochloride (GuHCl) concentration of the experimental data and fitted lines shown in Figure 8. For the fitted lines, $1/s$ was obtained from the fitted calculation. For the experimental data, $1/s$ was calculated by relating f_H (obtained by Equation (38)) to s, according to Equation (21). (**a**) C17 and (**b**) AK16. △ ($p=1$) and ◇ ($p=2$) show the experimental results of $1/s$. The broken line ($p=1$) and solid line ($p=2$) show the fitted lines of $1/s$. The insets show the relationship between Δ and v^2. $p=1$ (△), $p=2$ (◇).

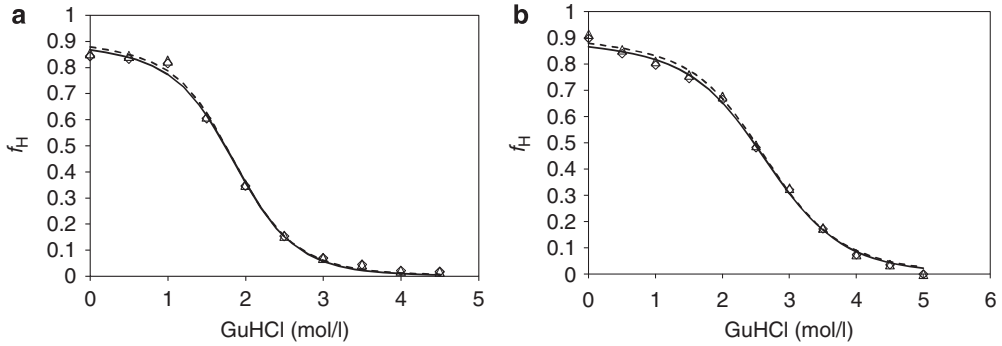

Figure 10 Calculated helix fractions (f_H) versus the guanidine hydrochloride (GuHCl) concentration with experimentally obtained data. The fitted curves were obtained at $v^2=10^{-4}$ and $p=1$ and 2. (**a**) C17 and (**b**) AK16. △ ($p=1$) and ◇ ($p=2$) are the f_H values, which were calculated from the experimental data with the simulated parameters. The broken line ($p=1$) and the solid line ($p=2$) represent the calculated f_H values, which were obtained with the parameters described in the Results section.

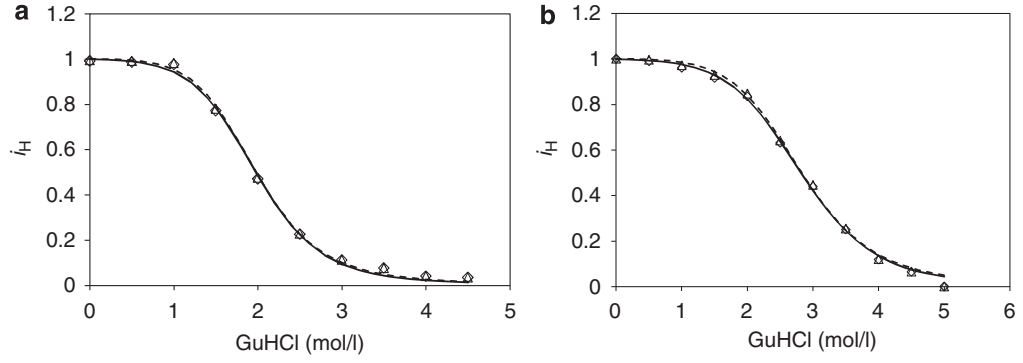

Figure 11 Calculated number of helices (i_H) versus the guanidine hydrochloride (GuHCl) concentration with experimentally obtained data. The fitted curves were obtained at $v^2=10^{-4}$ and $p=1$ and 2. (**a**) C17 and (**b**) AK16. △ ($p=1$) and ◇ ($p=2$) are the i_H values obtained from the experimental data with the simulated parameters. The broken line ($p=1$) and solid line ($p=2$) show the calculated i_H values, which were obtained with the parameters described in the Results section.

R_g of the complete helix can be expressed by the following equation:

$$R_g = \frac{1}{N}\sqrt{\sum_i \left(x_i - x_g\right)^2} = \frac{a}{N}\sqrt{\sum_i \left(i - \frac{1}{2} - \frac{N}{2}\right)^2} = \frac{a}{2}\sqrt{\frac{N^2-1}{3}} \quad (43)$$

where x_i is the coordinate of the i-th residue, x_g is the coordinate of the center of gyration and a is the projection length along the axis of the residue. The results indicated that $a=1.9$ Å, which is greater than the theoretical value of the α-helix (1.5 Å).[28] The calculation was conducted at $N=17$, and we assumed that all of the residues were present in the helical form.

R_g of the coiled state (Gaussian chain) can be expressed as[29]

$$R_g = \sqrt{\frac{N}{6}}b, \quad (44)$$

where b is the effective length per residue. These results indicated that $b=7.6$ Å. However, if the excluded volume effect is considered, the

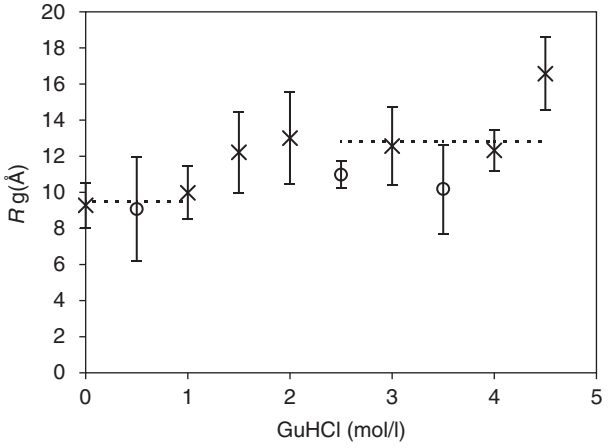

Figure 12 The dependence of R_g on the guanidine hydrochloride (GuHCl) concentration. ×: three times the experimental average; ○: two times the experimental average The straight broken lines represent the average R_g of the helix (0–1 mol l^{-1}) and the coiled form (2.5–4.5 mol l^{-1}).

value of b decreases. The transition from helix to coil was observed at denaturant concentrations of 1–2 mol l^{-1}, which coincides well with the CD results.

DISCUSSION

The effects of the denaturant concentration on the helix–coil transition have been treated thermodynamically by Schellman.[10,11] However, in the aforementioned derivation, intuitive treatment was implied. As shown in this study, statistical mechanics provide a satisfactory interpretation of the dependence of the helix–coil transition on the denaturant concentration, and detailed information was obtained.

As described in the Results section, the theoretical value of θ_{H0} for C17 and AK16 was $-29\,000$ (deg cm^{-2} $dmol^{-1}$) and $-22\,000$ (deg cm^{-2} $dmol^{-1}$), respectively. According to Scholtz *et al.*,[12] the value of θ_{H0} for peptides is approximately $-42\,500$ (deg cm^{-2} $dmol^{-1}$). Initially, we attempted to fit the data to a θ_{H0} value of $-40\,000$ (deg cm^{-2} $dmol^{-1}$); however, the simulation did not provide satisfactory results. Indeed, the value of θ for C17 is equal to $-36\,000$ (deg cm^{-2} $dmol^{-1}$) in excess trifluoroethanol (unpublished data). In this study, the experimental value of θ in the absence of GuHCl was $-25\,000$ (deg cm^{-2} $dmol^{-1}$) for C17 and $-20\,000$ (deg cm^{-2} $dmol^{-1}$) for AK16. These values remained unchanged as the proportion of methanol increased. The saturated CD value was solvent dependent, which suggests that the α-helix conformation may be dependent on the solvent.

The s_0 values reported by Scholtz *et al.*[12] are lower than those obtained in this study. Nevertheless, when the value of θ_{H0} was set to $-42\,500$ (deg cm^{-2} $dmol^{-1}$), the s_0 values were nearly identical to those obtained by Scholtz *et al.*;[12] however, the fitting was poor.

1 Zimm, B. H. & Bragg, J. K. Theory of the phase transition between helix and random coil in polypeptide chains. *J. Chem. Phy.* **31,** 526–531 (1959).
2 Nagai, K. Configuration change of polypeptide molecules. *J. Phys. Soc. Jpn.* **15,** 407–416 (1960).
3 Lifson, S. & Roig, A. On the theory of helix-coil transition in polypeptides. *J. Chem. Phys.* **34,** 1963–74 (1961).
4 Doig, A. J. Recent advances in helix-coil theory. *Biophys. Chem.* **101–102,** 281–293 (2002).
5 Poland, D. & Scheraga, H. A. *Theory of Helix-Coil Transitions in Biopolymers*, Academic Press, New York and London, 1970.
6 Tanford, C. Protein denaturation. *Adv. Protein Chem.* **23,** 121–282 (1968).
7 Tanford, C. Protein denaturation C. Theoretical models for the mechanism of denaturation. *Adv. Protein Chem.* **24,** 1–95 (1970).
8 Creighton, T. E. *Proteins: Structure and Molecular Properties*, (2nd edn.), (W.H. Freeman and Company, New York, 1993).
9 Fersht, A. *Structure and Mechanism in Protein Science*, (W. H. Freeman and Company, New York, 1998).
10 Schellman, J. A. Selective binding and solvent denaturation,. *Biopolymers* **26,** 549–559 (1987).
11 Schellman, J. A. A simple model for solvation in mixed solvents: applications to the stabilization and destabilization of macromolecular structures. *Biophys. Chem.* **37,** 121–140 (1990).
12 Scholtz, J. M., Barrick, D., York, E. J., Stewart, J. M. & Baldwin, R. L. Urea unfolding of peptide helices as a model for interpreting protein unfolding. *Proc. Natl. Acad. Sci. USA* **92,** 185–189 (1995).
13 De Gennes, P. G. Statistics of branching and hairpin helices for the dAT copolymer. *Biopolymers* **6,** 715–729 (1968).
14 Doi, M. Helix-coil transition under external forces. *Polymer J.* **6,** 222–229 (1974).
15 Kanô, F. Theory of the transition between the intra β-structure and the random coil in polyamino chains. *J. Phys. Soc. Jpn.* **41,** 219–227 (1976).
16 Kanô, F., Abe, I., Kamaya, H. & Ueda, I. A fractal model for adsorption on activated carbon surfaces: langmuir and Freundlich adsorption isotherms. *Surface Sci.* **467,** 131–138 (2000).
17 Doty, P. Configurations of biologically important macromolecules in solution. *Rev. Mod. Phys.* **31,** 107–117 (1959).
18 Kanô, F. & Doi, M. Dynamics of helix-coil transition and isotope exchange reaction. *J. Phys. Soc. Jpn.* **45,** 1354–1359 (1978).
19 Bixon, M. & Lifson, S. Solvent effect on the helix-coil transition in polypeptides. *Biopolymers* **4,** 815–821 (1966).
20 Teramoto, A. Helix-coil transition of polypeptides. *Seibutubutur* **13,** 149–163 (1973).
21 Amemiya, Y., Wakabayashi, K., Hamanaka, T., Wakabayashi, T. & Hashizume, H. Design of a small-angle X-ray diffractometer using synchrotron radiation at the photon factory. *Nucl. Instrum. Methods* **208,** 471–477 (1983).
22 Amemiya, Y., Ito, K., Yagi, N., Asano, Y., Wakabayashi, K., Ueki, T. & Endo, T. Large-aperture TV detector with a beryllium-windowed image intensifier for X-ray diffraction. *Rev. Sci. Instrum.* **66,** 2290–2294 (1995).
23 Ito, K., Kamikubo, H., Arai, M., Kuwajima, K., Amemiya, Y. & Endo, T. Calibration method for contrast reduction problem in the X-ray image-intensifier. *Photon Factory Activity Rep.* **18,** 275 (2001).
24 Ito, K., Kamikubo, H., Yagi, N. & Amemiya, Y. Calibration method and software for image distortion and non-uniformity in CCD-based X-ray detectors utilize X-ray image-intensifier. *Jpn. J. Appl. Phys.* **44** (Part 1), 8684–8691 (2005).
25 Pace, C. N. Determination and analysis of urea and guanidine hydrochloride d enaturation curves. *Methods Enzymol* **131,** 266–280 (1986).
26 Scholtz, J. M., Qian, H., York, E. J., Stewart, J. M. & Baldwin, R. L. Parameters of helix-coil transition theory for alanine-based peptides of varying chain lengths in water. *Biopolymers* **31,** 1463–1470 (1991).
27 Rohl, C. A., Scholtz, J. M., York, E. J., Stewart, J. M. & Baldwin, R. L. Kinetics of amide proton exchange in helical peptides of varying chain lengths. Inter pretation by the Lifson-Roig equation. *Biochemistry* **31,** 1263–1269 (1992).
28 Branden, C. & Tooze, J. *Introduction to Protein Structure* (Garland, New York and London, 1991).
29 Saito, N. *Koubunsi Butsurigaku* (Shokabo, Tokyo, 1967).